Hindawi
Advances in Civil Engineering
Volume 2019, Article ID 8097890, 11 pages
https://doi.org/10.1155/2019/8097890

Research Article

Comparison of Real Response and Theoretical Modeling of Pavement with Thick Asphalt Layers under Heavy Traffic Load

Jingsong Shan,[1] **Hongmei Shao**,[1] **Qiuzhong Li**,[2] **and Peili Sun**[3]

[1]*Shandong Key Laboratory of Civil Engineering Disaster Prevention and Mitigation, Shandong University of Science and Technology, Qingdao 266590, China*
[2]*Shandong Jinchao Engineering Test Co., Ltd., Jinan, China*
[3]*Jinan Urban Construction Group, Jinan 250031, China*

Correspondence should be addressed to Jingsong Shan; cyhsjs@163.com

Received 22 May 2019; Revised 2 August 2019; Accepted 12 August 2019; Published 3 September 2019

Academic Editor: Dimitris Rizos

Two kinds of asphalt pavement with thick asphalt layers were used to construct two samples. In structure I, a semirigid base and graded crushed stone subbase were used. In structure II, a granular base and semirigid subbase layer were used. Responses of the two structures under traffic loads were measured using optical fiber sensors, and the differences between theoretical model results and field measurements were analyzed. Field measurements show that vertical compressive stress in structure I is larger than that in structure II. The maximum tensile strain of the asphalt layer is located at the bottom of the AC-25C layer in structure I and at the bottom of the AC-25F layer in structure II. The latter is significantly larger than the former, indicating the possibility of fatigue cracking induced by traffic load is higher in structure II. The measured tensile horizontal strain at the bottom of the semirigid layer is relatively low ($<30\varepsilon\mu$) in both structure I and structure II. In theoretical model, static modulus, dynamic modulus, and interface bonding ability are considered and theoretical responses are calculated. There are significant differences between the theoretical results and field test data. In the theoretic model, the material properties of layers and bonding status of adjacent layers all influence the results. In order to reduce the difference between the calculated and measured results, numerous material tests and field tests should be carried out.

1. Introduction

Road paving materials and their mechanical properties are complicated. Ideal theory analysis cannot accurately reflect the true pavement response. So, theoretical calculation results should be revised to agree with pavement response data. In 1989, Mendez et al. proposed embedding fiber grating sensors (FBGs) in reinforced concrete to measure the status of the internal structure [1]. Then, in 1992, Prohaska et al. put FBG in reinforced concrete to measure strain [2]. FBG can also be used to measure asphalt pavement temperature [3]. A regression formula for pavement temperature was formed by combing field data and numerical analysis [4, 5]. Pavement temperature and response were measured, and a simulation model was created based on the field data [6, 7]. With the development of testing technology, pavement three-dimensional response could be tested and analyzed considering load magnitude and loading speed [8]. Vertical strains of the No. 40 Interstate Road in New Mexico, United States were tested, and test data and simulation data were compared [9–11]. In addition, GPR and core sampling were combined to determine the thickness of pavement layers, and the modulus of each layer was back-calculated using Falling Weight Deflectometer (FWD) data [12, 13].

In recent years, the mechanics-empirical method has been widely accepted for its connection between field measurements, theoretical calculation results, and pavement distresses. In the theoretical method, road material mechanical parameters must be tested and input into the theoretical model. Mechanical parameters have an important effect on the accuracy of the results [14–16].

Real pavement responses can be obtained directly in the field, but a significant amount of manpower and cost is required. On the other hand, theoretical calculations can be carried out easily by computers but are less accurate due to assumptions in the theoretical model. In this study, two types of asphalt pavement with thick asphalt layers are proposed and constructed. Real stress and strain responses in the pavement layers are tested, and the difference between the real responses and theoretical simulation results is analyzed.

2. Field Test of Pavement with a Thick Asphalt Layer under Traffic Load

2.1. Test Road. In many countries, the major materials used in flexible pavement include hot-mix asphalt (HMA), asphalt stabilized base, cement-treated base (CTB), other chemically treated materials (e.g., lime-fly ash, soil cement, lime-stabilized soils, etc.), and unbound aggregate base/subbase. In China, cement-stabilized material is widely used as the base and subbase layers. However, fatigue and reflective fracturing are inevitable if the chemically treated materials are used directly below asphalt layers. Unbound aggregate can restrain the reflective cracking progress, and thicker asphalt layers can also delay crack propagation within the asphalt layers.

Based on the above considerations, the pavement structures illustrated in Figures 1 and 2 are proposed as the test load structures. HMA layers with a total thickness of 30 cm are used. In structure I, cement-treated material is used as the base layer, and unbound granular aggregate is used as the subbase layer. Unlike structure I, an unbound aggregate layer is placed between the asphalt and cement-treated layers in structure II. The total thickness of pavement layers is 80 cm. In AC-25C and AC-25F, the symbols C and F denote either a coarse gradation or fine gradation, respectively.

2.2. Installation of FBG. FBGs have been used to measure pavement structure response in recent years [3]. FBGs are a kind of optical fiber passive component, which have higher accountability, higher accuracy, and less electromagnetic interference compared to other sensors. During construction of the test road, FBGs are placed within pavement layers (Figure 3). FBG installation should adhere to the following rules:

(1) According to the transverse distribution of vehicles, sensors should be placed underneath the wander of the traffic load to ensure the maximum pavement response is recorded.

(2) Two or more sensors are required at the same position to verify the data. If the data from the two sensors are significantly different, further analysis must be conducted.

(3) The distance between structure I and structure II should be as small as possible to link the transmission wire to a common point (Figure 3).

SMA-13	4 cm
AC-20C	6 cm
AC-25C	10 cm
AC-25F	10 cm
Cement treated base	34 cm
Granular subbase	16 cm
Subgrade	

Figure 1: Test road pavement structure I.

SMA-13	4 cm
AC-20C	6 cm
AC-25C	10 cm
AC-25F	10 cm
Granular base	16 cm
Cement treated subbase	34 cm
Subgrade	

Figure 2: Test road pavement structure II.

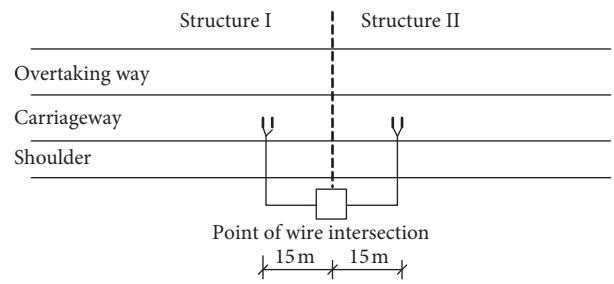

Figure 3: FBG layout.

All sensors and transmission wires must be protected during pavement construction. Grooves should be cut in the pavement first; then the FBG and wires are placed in the groove and covered with road material to ensure that the sensors and wires are protected (Figures 4 and 5). All sensors must be examined as soon as possible after construction to verify that the sensor is operable.

Three different types of sensors are used: compressive stress sensors, strain sensors, and temperature sensors (Table 1). Sensors are linked to a demodulator by fiber wires, and the wavelength variation of all sensors is recorded using the demodulator. Because the asphalt layer response is

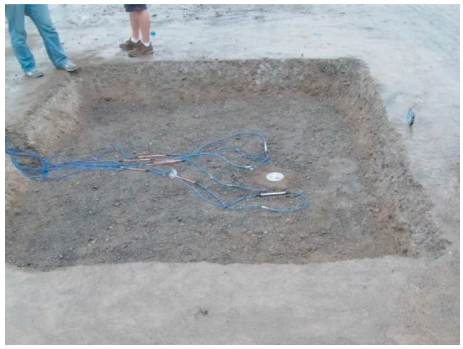

Figure 4: The instrument and landfill.

Figure 5: Protecting the FBG.

closely related to temperature, temperature sensors should be placed at the same position as the other sensors. Considering that sensors are easily destroyed by rollers during construction, test sensors are primarily placed in the AC-25C and underlying layers.

3. Field Data Processing

A heavily loaded truck was used as a test vehicle. The weight of the front and rear axles was 7.46 tons and 23.7 tons, respectively. Before the field test begins, a mark should be made on the road surface over the FBGs to ensure that the test vehicle passes directly over the FBGs. The test truck had a uniform speed of 60 km/h. A demodulator with a frequency of 100 Hz was used to collect wavelength data every 0.01 s. Pavement response can be calculated using the FBG wavelength variation using formulas (1) through (3):

$$P = K_1(\lambda_1 - \lambda_0), \quad (1)$$

$$\varepsilon = K_2(\lambda_1 - \lambda_0), \quad (2)$$

$$T = K_3(\lambda_1 - \lambda_0), \quad (3)$$

where P is the vertical compressive stress, ε is the horizontal strain, K_1 is the stress coefficient (kPa/nm), K_2 is the strain coefficient ($\mu\varepsilon$/nm), K_3 is the temperature coefficient (°C/nm), λ_1 is the current wavelength of FBG (nm), and λ_0 is the initial wavelength of FBG (nm)

3.1. Vertical Compressive Stress. The vertical compressive stress vs. time for structures I and II are plotted in Figures 6 and 7, respectively. When the test vehicle passes over the test sensors, the vertical stress response is calculated and recorded. The compressive stress response in the two structures is similar. Two wave peaks resulting from the front and rear axles, respectively, are visible. The response induced by the rear axle is significantly larger than the front axle response because the load magnitude of the rear axle is significantly larger than the front axle.

The compressive vertical stress in structure I is larger than that in structure II at the same position. For instance, the peak vertical compressive stress at the top of the AC-25F layer is 338.0 kPa in structure I; however, the peak vertical compressive stress is 206.3 kPa in structure II. The former is 1.64 times larger than the latter.

In Figure 7, the compressive stress response at the granular layer top is plotted. The peak of vertical stress in structure I is 43.0 kPa, which is much less than structure II (169.0 kPa). The difference comes from the granular layer depth. The distance from the granular layer top to pavement surface is 64 cm in structure I; however, this distance is 30 cm in structure II. Therefore, it can be concluded that the semirigid layer transfers and spreads the traffic load well and reduces the possibility of deformation in the granular layer.

3.2. Horizontal Strain. Horizontal strain in the pavement layers is plotted in Figures 8–10, from which several conclusions can be drawn:

(1) The horizontal strain response in structures I and II are similar when the traffic load passes over the test sensors. Horizontal strains are compressive at the bottom of the AC-25C and AC-25F layers when the test vehicle is not directly over an FBG; however, when the test vehicle is directly over an FBG, the horizontal strain is extensional.

(2) The tensile strain in structure II is significantly larger than that in structure I. For example, the maximum tensile strain at the bottom of the AC-25C layer in structure I is 118$\varepsilon\mu$ and 160$\varepsilon\mu$ in structure II. The maximum tensile strain beneath the AC-25F layer in structure I is 60$\varepsilon\mu$ and 283$\varepsilon\mu$ in structure II. As a result, fatigue cracking may be more likely in structure II.

(3) The position of the maximum strain is different in structure I and structure II. The point of maximum tensile strain is at the bottom of the AC-25C layer in structure I but is located at the bottom of the AC-25F layer in structure II.

(4) In structure I and structure II, tensile strain exists beneath the cement stabilized layer; however, the tensile strain magnitude at the bottom of cement stabilized layer is small. Thus, fatigue cracking is less likely in CTB with a thick asphalt layer and thick CTB base layer.

Table 1: FBG layout.

Test channel	Sensor number	Initial wavelength (nm)	Sensor type	Position	Structure type
Channel one	1-YB-1/1-YB-2	1561.28/1562.65	Strain	Bottom of AC-25F	Structure I
Channel two	2-YB-1/2-YB-2	1557.507/1558.91	Strain	Bottom of AC-25C	
	2-T-1	1529.092	Temperature	Bottom of SMA	
Channel three	3-CS-1/3-CS-2	1550.05/1548.63	Pressure	Top of CTB layer	
	3-CS-3/3-CS-4	1562.994/1564.31	Pressure	Top of granular base	
	3-CS-5/1-CS-6	1557.768/1555.923	Pressure	Bottom of AC-25C	
Channel four	4-YB-1/4-YB-2	1539.382/1538.102	Strain	Bottom of CTB	
	5-T-1	1552.834	Temperature	Bottom of AC-25F	
Channel five	5-YB-1/5-YB-2	1557.569/1554.43	Strain	Bottom of AC-25F	
	5-T-2	1544.588	Temperature	Bottom of AC-20C of AC25-C	
Channel six	6-YB-1/6-YB-2	1541.914/1542.723	Strain	Bottom of CTB	Structure II
	6-YB-3/6-YB-4	1545.33/1547.62	Strain	Bottom of AC-25F	
	6-YB-5/6-YB-6	1550.016/1548.012	Strain	Bottom of AC-25F	
Channel seven	7-CS-1/7-CS-2	1545.966/1544.827	Pressure	Bottom of AC-25C	
	7-YB-1/7-YB-1	1557.584/1556.791	Strain	Bottom of AC-25C	
	7-T-1	1553.012	Temperature	Bottom of SMA	
	7-T-2	1544.609	Temperature	Bottom of AC-25F	
Channel eight	8-T-1	1544.693	Temperature	Bottom of AC-20C	
	8-CS-1/8-CS-2	1537.951/1539.832	Pressure	Top of granular base	

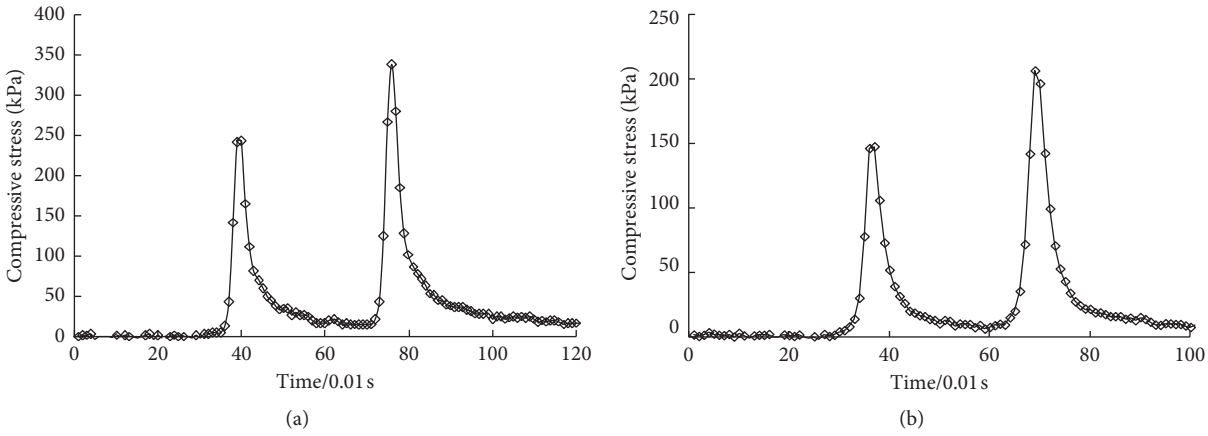

Figure 6: Vertical compressive stress at the top of AC-25F. (a) Structure I. (b) Structure II.

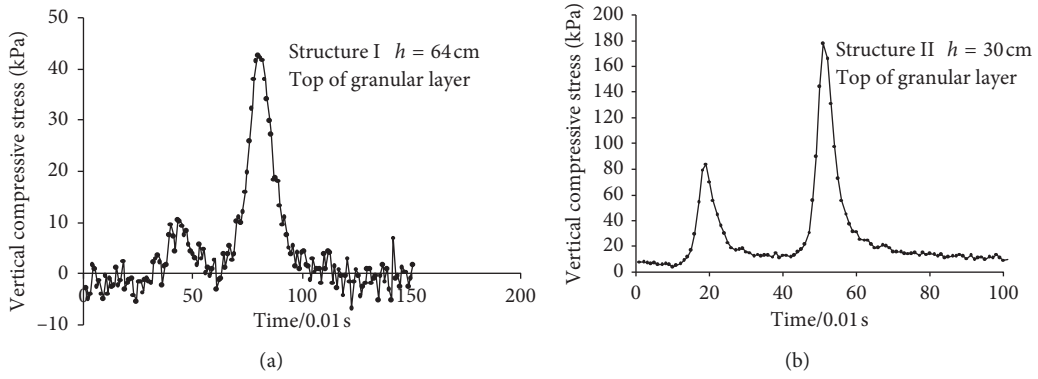

Figure 7: Vertical compressive stress at the top of the granular layer. (a) Structure I. (b) Structure II.

3.3. Temperature in Asphalt Layers. Field tests were conducted from 10 am to 12 am on a sunny day without wind and an atmospheric temperature of 29.2°C. Temperature in the asphalt layers during the test period is plotted in Figure 11. Temperature fluctuation exists at the test point, but fluctuations are not greater than 1°C. The

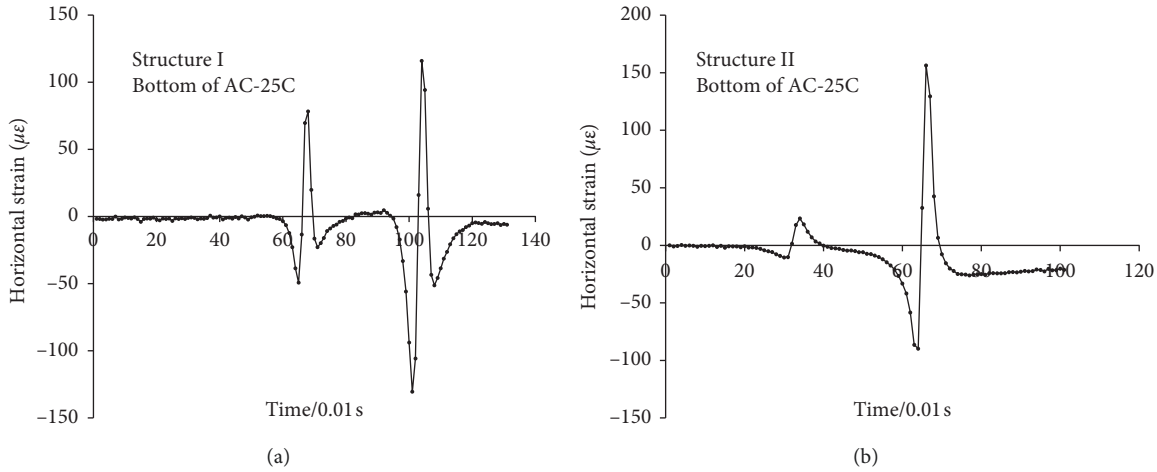

Figure 8: Horizontal strain at the bottom of AC-25C.

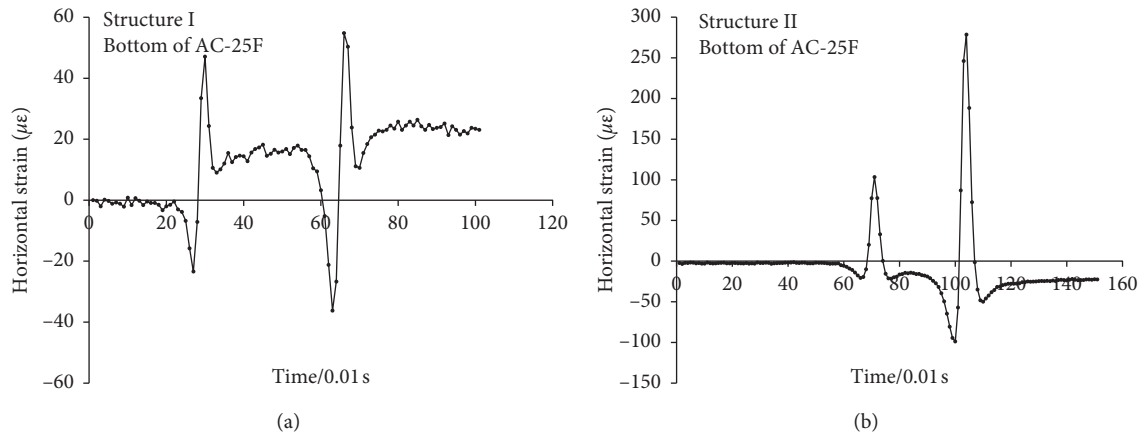

Figure 9: Horizontal strain at the bottom of AC-25F.

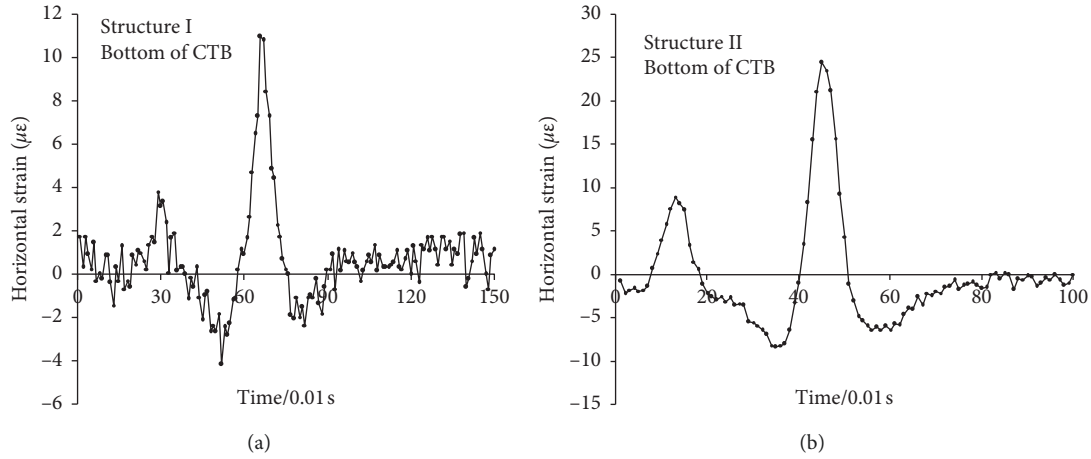

Figure 10: Horizontal strain at the bottom of the cement-stabilized base.

average temperature during the test is regarded as the representative temperature at the moment of testing. The temperature at the bottom of the SMA ($h = 4$ cm), AC-20 ($h = 10$ cm), AC-25C ($h = 20$ cm), and AC-25F ($h = 30$ cm) layers was 39.3°C, 34.6°C, 25.5°C, and 24.7°C, respectively.

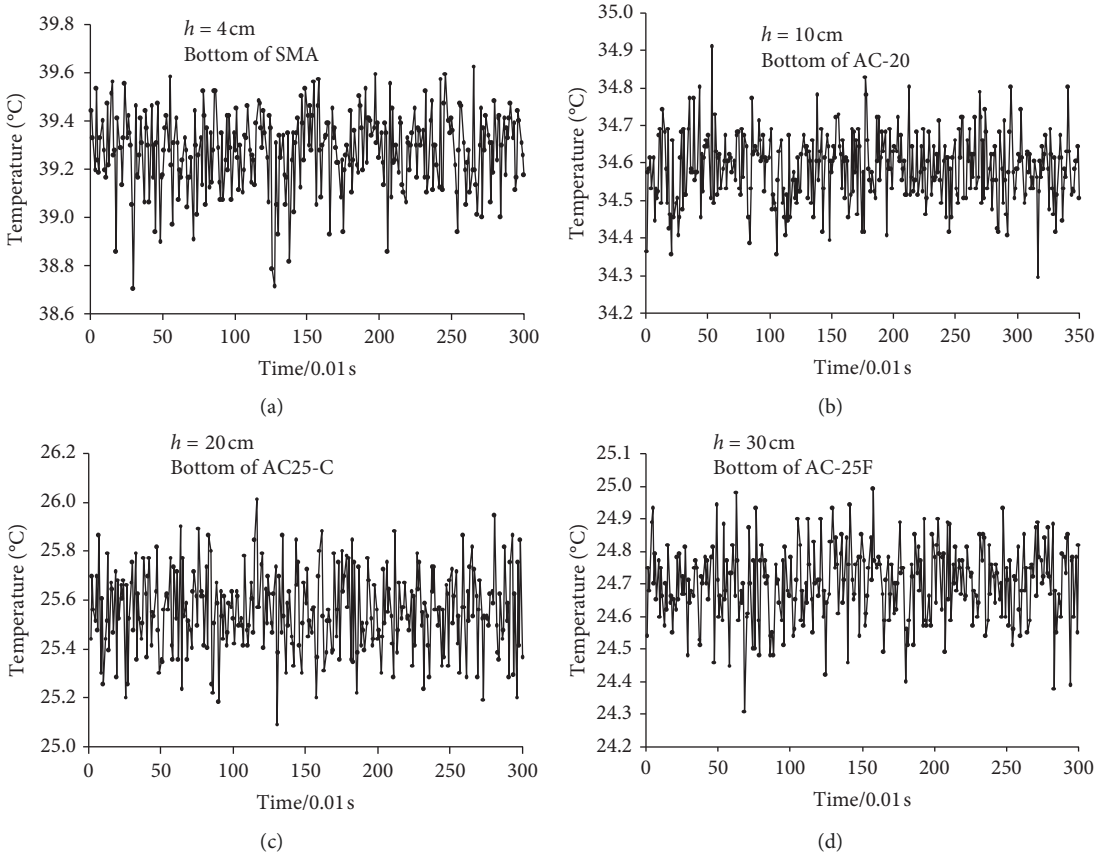

Figure 11: Measured temperatures in asphalt layers. (a) $h = 4$ cm, (b) $h = 10$ cm, (c) $h = 20$ cm, and (d) $h = 30$ cm.

4. Comparison of Theoretical Results and Field Data

Although field tests can help to obtain the real inner responses of pavement structures, field tests have some limitations. For instance, the subgrade condition, pavement structure, and testing method can all have an effect on test data, which results in difficulty directly applying test results to pavement design. Field tests are also expensive and time consuming. By comparison, theoretical analysis is cheaper and faster. The following paragraphs focus on comparing theoretical results and field test results in order to improve the accuracy of the theoretic results.

In the theoretic model, road pavement is assumed to be composed of multiple elastic layers characterized by an elastic modulus and Poisson's ratio. In this section, the effects of material properties including static modulus, dynamic modulus, and interface contact conditions between layers are analyzed.

4.1. Test Truck Load Parameters. The contact parameters between the test truck's tire and road surface are calculated listed in Table 2 and are used as inputs for the theoretic model [17].

4.2. Influence of Static Modulus. Static modulus is widely used in theoretic modeling. Asphalt layer modulus is determined using the real temperature of the test road in Figure 11. Because the temperature in the AC-25F and AC-25C layers is similar, the static modulus of the two layers is set to same value. In order to analyze the influence of asphalt modulus on the theoretic model, the modulus of the AC-25C and AC-25F layers is varied while the modulus of other layers is held constant. Three modulus combinations are listed in Table 3.

Table 2: Parameter of test vehicle.

Rear axle load of test vehicle P (kN)	237
Weight of single wheel (kN)	59.25
Contact pressure of tire (MPa)	0.948
Contact area (cm^2)	626
Equivalent diameter of single wheel d (cm)	28.2
Center-to-center distance of two wheels (cm)	$1.5d$

Variations in asphalt layer modulus have a small effect on the theoretical vertical compressive stress (Figure 12). The theoretical compressive vertical stresses in structures I and II are both significantly larger than the corresponding field measurements. For example, compressive vertical stresses at the bottom of the AC-25C and AC-25F layers in structure I are 62.3% and 58.7% larger than the respective measured values. The compressive vertical stresses at the bottom of the AC-25C and AC-25F layers in structure II are 45.8% and 70.1% larger than the respective measured values. The differences between the theoretic and real responses have nothing to do with the asphalt layer static modulus.

Table 3: Static modulus.

Pavement layers	Modulus (MPa) combination I	Modulus (MPa) combination II	Modulus (MPa) combination III	Poisson's ratio
SMA-13	450	450	450	0.25
AC-20	700	700	700	0.25
AC-25C, AC-25F	**800**	**1000**	**1200**	0.25
CTB	1400	1400	1400	0.20
Granular	400	400	400	0.25
Subgrade	40	40	40	0.3

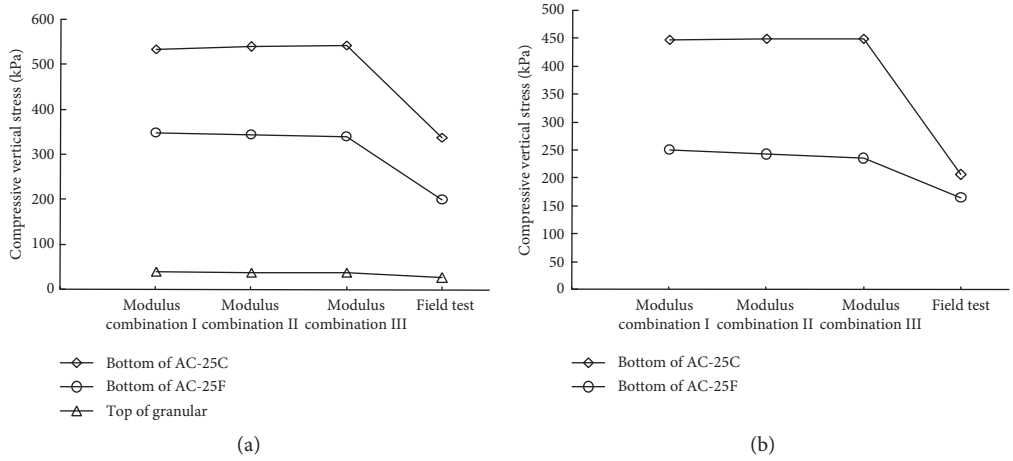

Figure 12: Comparison of theoretical vertical stress and measured vertical stress. (a) Structure I. (b) Structure II.

The theoretical tensile strains at the bottom of the AC-25C and AC-25F layers are significantly smaller than the measured values (Figure 13). The theoretic horizontal strain at the bottom of the cement treated layer is significantly larger than the corresponding field measurement. With increasing asphalt layer modulus, theoretic tensile strain at the bottom of the AC-25C layer in structure I decreases, but the tensile strain in the AC-25F layer increases slightly. In structure II, tensile strain in the AC-25C layer decreases with increasing asphalt layer modulus, similar to structure I, and the tensile strain at the bottom of the AC-25F layer shows little change. It should be noted that the tensile horizontal strain in asphalt layers may be underestimated, and the tensile strain at the bottom of the CTB layer may be significantly overestimated when the theoretic method is used. Thus, the theoretical results should be revised before applying them to pavement design.

4.3. Influence of Semirigid Layer Modulus. In order to analyze the influence of semirigid layer modulus on pavement response, the modulus of all asphalt layers in the theoretical model were fixed, and only the semirigid layer modulus was varied. The modulus of the AC-25C and AC-25F layers were fixed at 1000 MPa, and the modulus of CTB layer was varied from 1000 MPa to 1800 MPa. The parameters of the other layers are listed in Table 3.

Variation in the CTB base or subbase modulus has little effect on the compressive vertical stress of pavement layers (Table 4). However, varying the semirigid layer modulus can influence the tensile strain of asphalt layers (Table 5). With increasing CTB modulus, tensile strains at the bottom of the AC-25C and AC-25F layers decrease, especially in the AC-25F layer. Increasing the CTB layer modulus is conducive to reducing the possibility of fatigue cracking beneath asphalt layers under traffic load. However, it must be noted that the discrepancy between theoretic results and field measurements will grow with increasing CTB modulus in the theoretic model.

4.4. Influence of Asphalt Layer Dynamic Modulus. The dynamic modulus of asphalt mixtures can be tested using laboratory methods, and results were related to loading rate and temperature [18, 19]. In this study, the dynamic modulus of asphalt layers is determined based on past studies. The dynamic modulus of asphalt mixtures under a loading frequency of 10 Hz is listed in Table 6. The theoretical results are listed in Table 7.

Theoretical results show that if dynamic modulus is used, the compressive vertical stresses in the asphalt layers are clearly less when using the static modulus. The difference between theoretical compressive stress and measured data decreases when the dynamic modulus is adopted in the theoretical model.

The maximum tensile horizontal strain positions appear at the bottom of the AC-25F layer in both structure I and structure II when the dynamic modulus is used in the theoretical model. The maximum tensile strain of asphalt layers in structure II decreased significantly compared with the calculated results using the static modulus model. Thus, the dynamic modulus has a greater effect on the theoretical strain response of structure II.

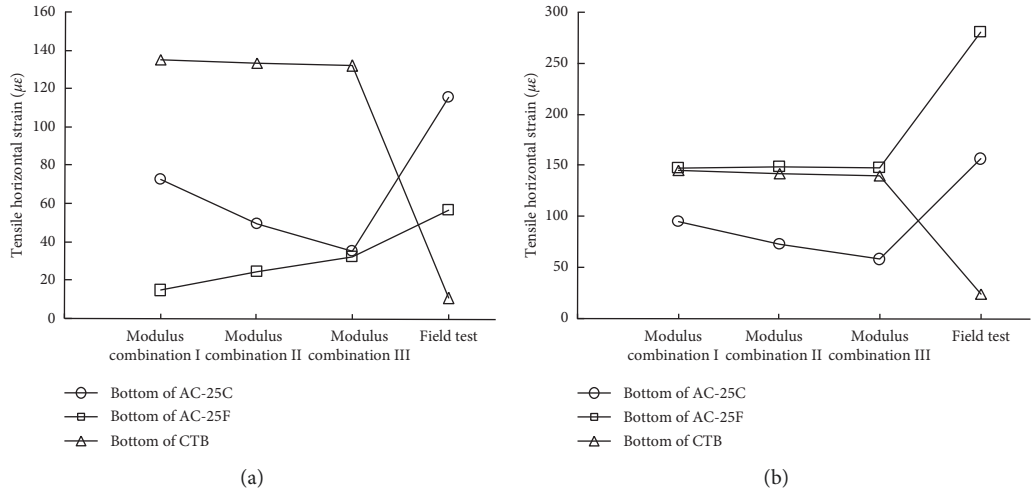

Figure 13: Comparison of theoretical horizontal tensile strain and measured tensile strain. (a) Structure I. (b) Structure II.

Table 4: Compressive vertical stress.

	Position	Compressive vertical stress (kPa)			
		Modulus (MPa) combination I	Modulus (MPa) combination II	Modulus (MPa) combination III	Field measured (MPa)
Structure I	AC-25C	524.5	539.7	549.8	338.0
	AC-25F	325.1	344.5	357.8	199.6
	CTB	42.3	38.7	35.9	39.6
Structure II	AC-25C	446.2	450.0	451.9	206.6
	AC-25F	237.0	243.3	247.6	165.4

Table 5: Tensile horizontal strain.

	Position	Tensile horizontal strain ($\mu\varepsilon$)			
		Modulus (MPa) combination I	Modulus (MPa) combination II	Modulus (MPa) combination III	Measured values
Structure I	AC-25C bottom	56.0	49.8	47.6	115.9
	AC-25F	62.1	24.9	3.8	56.8
	CTB	145.7	133.6	123.5	10.9
Structure II	AC-25C bottom	73.1	72.9	72.5	156.3
	AC-25F	157.5	149.0	144.3	280.6
	CTB	167.9	142.5	125.7	24.4

Table 6: Asphalt dynamic modulus.

	Real temperature (°C)	Dynamic modulus (MPa)	Poisson's ratio
SMA-13	39.4	1900	0.25
AC-20	34.5	5500	0.25
AC-25C	25.5	10000	0.25
AC-25F	24.6	10500	0.25

On the whole, using the dynamic modulus leads to a decreased theoretical compressive stress and tensile strain in asphalt layers. As a result, the difference between theoretical vertical compressive stress and field measurements is reduced and the difference in tensile strains is increased.

4.5. Interface between the Asphalt Layer and Base Layer. When pavement structures are constructed, the interface between layers may be not fully bonded because the adjacent materials are not same. Bonding conditions are considered in the theoretical model to analyze the effect of interface characteristics on pavement response. Only the bonding

Table 7: Theoretical results.

Structure type	Position	Compressive vertical stress (kPa)		Tensile horizontal strain ($\mu\varepsilon$)	
		Theoretical	Field test	Theoretical	Field test
Structure I	AC-25C	437.7	338.0	8.0	115.9
	AC-25F	190.3	199.6	54.1	56.8
	CTB	23.2	39.6	83.5	10.9
Structure II	AC-25C	380.5	206.6	10.1	156.3
	AC-25F	150.5	165.4	66.0	280.6
	CTB			85.7	24.4

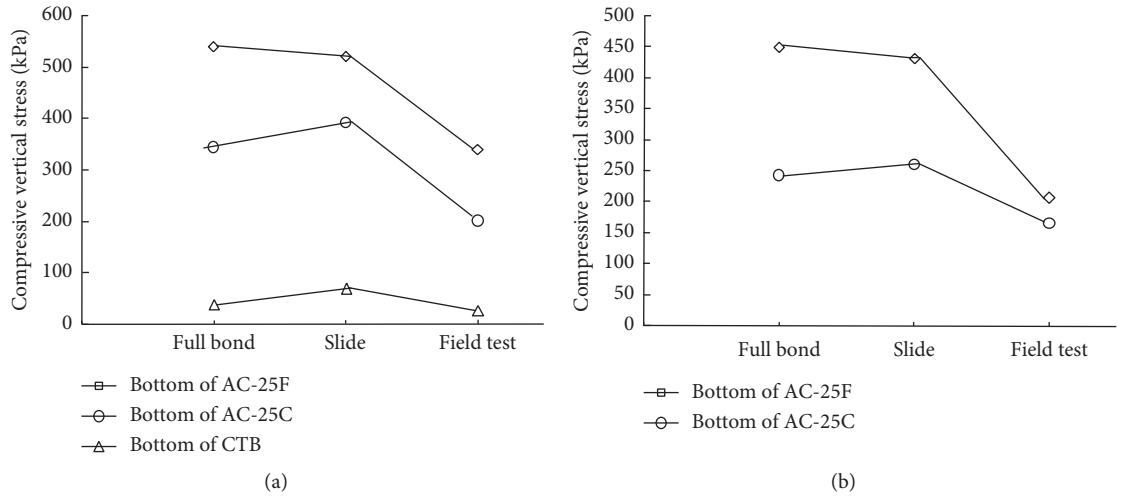

Figure 14: Effect of bonding condition on compressive vertical stress. (a) Structure I. (b) Structure II.

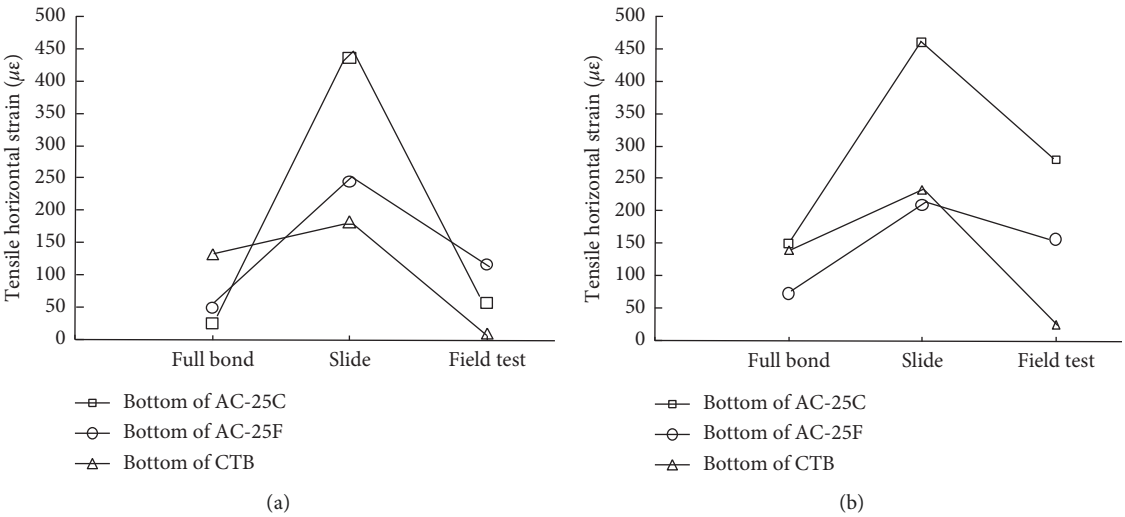

Figure 15: Effect of bonding condition on tensile horizontal strain. (a) Structure I. (b) Structure II.

status between the lowest asphalt layer and base layer is considered, including a fully bonded boundary and a sliding boundary (Figures 14 and 15).

The bonding conditions between the asphalt and base layers have the same effect on the compressive vertical stress in structure I and structure II. The sliding boundary led to an increased compressive vertical stress in the AC-25F layer and decreased compressive vertical stress in the AC-25C layer. Overall, the change in compressive vertical stress magnitude is not significant. In contrast, the effects of interface condition on tensile horizontal strain are significant. For a sliding boundary, the theoretical tensile horizontal strains of the AC-25C and AC-25F layers in structure 1 are 3.9 times and 16.5 times larger, respectively, compared to a

fully bonded layer. In structure 2, the increase ratio of tensile horizontal strain is 1.9 times and 2.1 times, respectively.

The theoretical horizontal strain in asphalt layers is larger than field measurements for a sliding boundary. However, if the boundary is fully bonded, the theoretical results will be less than field measurements. Thus, the interface type has an important effect on the theoretical results. It is necessary to reasonably evaluate the actual interface type in order to decrease the difference between theoretical and real responses.

5. Conclusion

In this study, two kinds of pavements with thick asphalt layers are designed and used to construct test road samples. The responses of pavement layers under traffic loading are measured. The differences between the theoretical results and field measurements are analyzed, and several conclusions are drawn as follows:

(1) According to field data, the compressive vertical stress in the asphalt layers of structure I is larger than in structure II at the same depth, indicating that the asphalt material in structure I undergoes more severe compression under traffic load.

(2) The position of the maximum horizontal tensile strain in structure I is located at the bottom of the AC-25C layer. The same point is located at the bottom of the AC-25F layer in structure II, and the magnitude of maximum horizontal tensile strain is 2.42 times larger in structure II than in structure I based on field data, indicating fatigue cracking is more likely to occur in structure II with a granular base layer.

(3) The measured tensile strains of a semirigid base layer are relatively low (less than $30\mu\varepsilon$), indicating that fatigue cracking induced by traffic load may not initiate at the bottom of the CTB covered with a thick asphalt layer.

(4) Pavement responses calculated using the theoretical model are distinctly different from field measurements. Theoretical compressive vertical stresses are significantly larger than field measurements, and the theoretical tensile strain in asphalt layers is significantly less than field measurements if the interface condition is good. Thus, the predicted service life of pavement will deviate from the actual service life if the theoretical response is directly used to design the pavement.

(5) Material properties and interface bonding condition have significant effects on theoretical pavement response. It is difficult to reduce the difference between theoretical results and field measurements only by varying the material modulus of certain layers or one interface bonding condition. Numerous material tests and field tests must be conducted in order to establish a reasonable relationship between theoretical results and field measurements.

Data Availability

The authors declare that all the data supporting the conclusions of the present study can be obtained from the corresponding author.

Conflicts of Interest

There are no conflicts of interest regarding the publication of this article.

Authors' Contributions

Jingsong Shan and Hongmei Shao designed the field test. QiuZhong Li and Peili sun performed the field test. Jingsong Shan conducted the theoretical analysis. Hongmei Shao analyzed the field test data and wrote the paper.

Acknowledgments

This research was funded by the Project of Shandong Province Higher Educational Science and Technology Program, grant no. J17KA213.

References

[1] A. Mendez, T. F. Morse, and F. Mendez, "Applications of embedded optical fiber sensors in reinforced concrete buildings and structures," *Proceedings of the SPIE*, vol. 1170, pp. 60–69, 1990.

[2] J. D. Prohaska, E. Snitzer, B. Chen, M. H. Maher, E. G. Nawy, and W. W. Morey, "Fiber optic bragg grating sensor in large scale concrete structures," *Proceedings of the SPIE*, vol. 1798, pp. 1–22, 1993.

[3] D. Ze-jiao, L. Sheng-long, W. Jia-yu, and L. Zhen, "Real-time temperature field measurement of asphalt pavement based on fiber bragg grating measuring technology," *Journal of Traffic and Transportation Engineering*, vol. 14, no. 2, pp. 1–6, 2014, in Chinese.

[4] Y. Xi-li, Z. Shi-ping, L. Yan, and H. Xiao-yuan, "Analysis of temperature field of asphalt pavement by site measurement in full-depth," *Journal of Chang'an University: Natural Science Edition*, vol. 36, no. 1, pp. 1–7, 2016, in Chinese.

[5] K. Hai-gui, Z. Yuan-xun, C. Ying-chun, and L. Yan, "Regression analysis of actual measurement of temperature field distribution rules of asphalt pavement," *China Journal of Highway and Transport*, vol. 20, no. 6, pp. 13–18, 2016, in Chinese.

[6] G. Xing-yu, Y. Qing-quan, and N. Fu-jian, "Analysis of factors on asphalt pavement rut development based on measured load and temperature gradient," *China Journal of Highway and Transport*, vol. 25, no. 6, pp. 30–36, 2012, in Chinese.

[7] H. Xiaodi and S. Lijun, "Stress response analysis of asphalt pavement under measured tire ground pressure of Heavy vehicle," *Journal of Tongji University: Natural Science*, vol. 34, no. 1, pp. 64–68, 2006, in Chinese.

[8] Z. J. Dong, H. Liu, Y. Q. Tan et al., "Field measurement of three-direction strain response of asphalt pavement," *Journal of South China University of Technology: Natural Science Edition*, vol. 37, no. 7, pp. 46–51, 2009, in Chinese.

[9] M. D. R. Islam and R. A. Tarefder, "Field measurement of vertical strain in asphalt concrete," *International Journal of Scientific & Engineering Research*, vol. 4, no. 2, pp. 1–6, 2013.

[10] M. D. R. Islam, M. U. Ahmed, and R. A. Tarefder, "Evaluation of the FWD moduli of a flexible pavement using finite element model," *International Journal of Civil, Environmental, Structural, Construction and Architectural Engineering*, vol. 7, no. 1, pp. 94–98, 2013.

[11] AASHTO, "Mechanistic-empirical pavement design guide," in *A Manual of Practice, AASHTO*, pp. 163–184, American Association of State Highway and Transportation Officials, Washington, DC, USA, Interim edition, 2008.

[12] J. Domitrović and T. Rukavina, "Application of GPR and FWD in assessing pavement bearing bearing capacity," *Romanian Journal of Transport Infrastructure*, vol. 2, no. 2, pp. 11–21, 2013.

[13] M. Ožbolt, T. Rukavina, and J. Domitrović, "Comparison of pavement layer thickness measured by GPR and conventional methods," *The Baltic Journal of Road and Bridge Engineering*, vol. 7, no. 1, 2012.

[14] J. Zhang, J. Peng, J. Zheng, L. Dai, and Y. Yao, "Prediction of resilient modulus of compacted cohesive soils in South China," *International Journal of Geomechanics*, vol. 19, no. 7, Article ID 04019068, 2019.

[15] J. Li, J. Zhang, G. Qian, J. Zheng, and Y. Zhang, "Three-dimensional simulation of aggregate and asphalt mixture using parameterized shape and size gradation," *Journal of Materials in Civil Engineering*, vol. 31, no. 3, Article ID 04019004, 2019.

[16] J. Zhang, J. Li, Y. Yao, J. Zheng, and F. Gu, "Geometric anisotropy modeling and shear behavior evaluation of graded crushed rocks," *Construction and Building Materials*, vol. 183, pp. 346–355, 2018.

[17] W. Heukelom and A. J. G. Klomp, "Dynamic testing as a means of controlling pavements during and after construction," in *Proceedings of the International Conference on the Structural Design of Asphalt Pavements*, pp. 667–679, Ann Arbor, MI, USA, August 1962.

[18] J. Shan and S. Wu, "Analysis of rutting resistance of asphalt pavement," *Journal of Building Materials*, vol. 19, no. 3, pp. 124–130, 2016, in Chinese.

[19] W. Jincheng, S. Cui, and J. Hu, "Research on dynamic modulus of asphalt mixtures," *Journal of Building Materials*, vol. 11, no. 6, pp. 657–661, 2008, in Chinese.